Optics Letters

Subattosecond x-ray Hong–Ou–Mandel metrology

SERGEY VOLKOVICH AND SHARON SHWARTZ*

Physics Department and Institute of Nanotechnology, Bar-Ilan University, Ramat Gan 52900, Israel
**Corresponding author: sharon.shwartz@biu.ac.il*

Received 6 November 2019; revised 22 March 2020; accepted 30 March 2020; posted 3 April 2020 (Doc. ID 382044); published 6 May 2020

We show that subattosecond delays and subangstrom optical path differences can be measured by using Hong–Ou–Mandel interference measurements with x-rays. Our scheme relies on the subattosecond correlation time of photon pairs that are generated by x-ray spontaneous parametric down-conversion, which leads to a dip in correlation measurements with a comparable width. Therefore, the precision of the measurements is expected to be better than 0.1 attosecond. We anticipate that the scheme we describe in this work will lead to the development of various techniques of quantum measurements with ultra-high precision at x-ray wavelengths. © 2020 Optical Society of America

https://doi.org/10.1364/OL.382044

Since its first observation [1], the Hong–Ou–Mandel (HOM) effect has attracted much attention due to its importance for fundamental quantum sciences and since it holds a great promise for new quantum technologies [2–14]. The HOM effect is a quantum effect that is based on the interference of the wave functions of the photons rather than on the interference of classical waves. The striking consequence of this quantum interference is manifested when two indistinguishable photons arrive simultaneously at the two different input ports of a 50:50 beam splitter. In contrast to classical waves, the two photons will always be detected at the same output port of the beam splitter. As a result, coincidence measurements between the output ports are null as long as the photons at the two input ports are indistinguishable.

In a typical HOM experiment, two identical photons are generated and propagate along two paths. By varying one of the optical paths, it is possible to control the delay between the two photons so that they do not arrive at the beam splitter simultaneously and their distinguishability is raised. The more distinguished the photons become, the higher the probability of coincident detection gets. The ability of the HOM effect to detect the indistinguishability of photons on very short time scales has led to the development of various approaches based on the effect for the measurements of ultrashort delays and optical path differences [15–18]. Measurements based on the HOM effect are more sustainable than measurements with classical interferometers, because unlike classical interferometers, HOM measurements are independent of the phase fluctuations of the optical beams. Consequently, in recent years several schemes for subfemtosecond delay measurements with optical beams have been suggested and implemented [16,17].

Generally, the extension of quantum optics to the x-ray regime can provide new and intriguing opportunities. This is especially due to the availability of photon number resolving detectors demonstrating high detection efficiencies and negligible background noise. X-rays are also more penetrative than optical photons, and as they possess higher frequencies, they can be modulated to carry more information. We note that several works on x-ray quantum effects have been reported recently [19–28].

To reap the benefits of extending the HOM effect to the x-ray regime, a key requirement is a source that produces identical photons. One prominent candidate source is based on spontaneous parametric down-conversion (SPDC), where a pump photon interacts with the vacuum field in a nonlinear crystal to generate two photons (biphotons) [29]. The keV bandwidth that has been reported for x-ray SPDC [20,30] suggests that the corresponding biphoton correlation time is on the order of a few attoseconds. Implementing the x-ray HOM effect can lead to the development of quantum optical coherence tomography for measurements of very short spatial scales and tiny refractive index differences [31–33]. This would be appealing for the imaging of biological samples.

However, the possibility to measure such a broad spectrum HOM effect is not clear. The main challenge is that x-ray mirrors and beam splitters rely either on small angle reflection or on Bragg scattering [34]. Small angle reflection can be used to reflect a very broad spectrum, but the angular distribution of the generated photons is much broader than the acceptance angle of small angle reflection devices. Bragg scattering from crystals is narrow in both angle and spectrum; thus, the HOM effect would be narrowband and the corresponding dip in the coincidence count rate would be limited to a few femtoseconds. The alternative is to use Bragg scattering from artificial periodic structures made by multilayers. However, it is not clear whether the technical feasibility of the present-day technology allows the fabrication of such a system. It is also not clear *a priori* that the photons that hit upon the two input ports of the beam splitter are indeed indistinguishable.

In this Letter, we describe a system that is based on available technologies for measuring the HOM effect at x-ray wavelengths. We show that when the photons hit the beam splitter simultaneously, they are indeed indistinguishable; hence, the

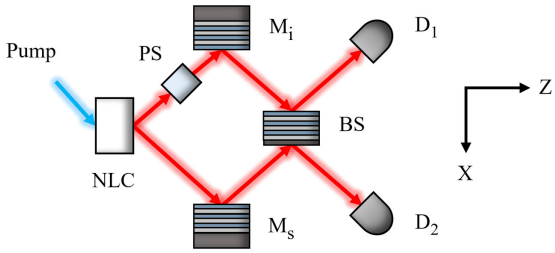

Fig. 1. Schematic diagram of the proposed experimental system. The pump photons are converted in a nonlinear crystal (NLC) into signal and idler photon pairs, and the idler enters a phase shifter (PS). The biphotons are then reflected by their corresponding multilayer mirrors (M_i and M_s) into a beam splitter (BS), and the coincidence count rate at its output is measured by two detectors (D_1 and D_2).

system can support the detection of very short delays. We consider an example where the full width half-maximum (FWHM) of the dip is about 0.6 attoseconds and explain how to control it.

We consider a standard scheme for HOM effect experiments that consists of a nonlinear crystal for the generation of x-ray biphotons, a phase shifter, two multilayer mirrors, and a multilayer beam splitter, as shown in Fig. 1. The biphotons emerging from the nonlinear crystal are commonly denoted as the "signal" and the "idler." This process is parametric; hence, energy is conserved and $\hbar\omega_p = \hbar\omega_s + \hbar\omega_i$, where ω_p, ω_s, and ω_i are the angular frequencies of the pump, signal, and idler photons, respectively. The signal and idler propagate at different directions, which are symmetric with respect to the symmetry axis determined by the momentum conservation (phase matching) of the process. Since all relevant wavelengths are on the order of the distance between the atomic planes of the generating crystal, phase matching is achieved via the reciprocal lattice vector $\boldsymbol{G}$ [35]. This leads to the condition $\boldsymbol{k}_p + \boldsymbol{G} = \boldsymbol{k}_s + \boldsymbol{k}_i$, where $\boldsymbol{k}_p$, $\boldsymbol{k}_s$, and $\boldsymbol{k}_i$ are the wave vectors of the pump, signal, and idler, respectively. One of the biphotons travels through a phase shifter and each of them is reflected by a mirror and impinges upon the opposite side of a beam splitter.

The generation of the biphotons in the nonlinear crystal is described by the frequency domain coupled equations for the signal and idler envelope ladder operators in the Heisenberg picture for a lossless medium [20,30]. By using the undepleted pump and the slowly varying envelope approximations we obtain

$$\frac{\partial \hat{a}_s}{\partial z} = \kappa \hat{a}_i^\dagger \exp(i\Delta k_z z), \qquad \frac{\partial \hat{a}_i^\dagger}{\partial z} = \kappa^* \hat{a}_s \exp(-i\Delta k_z z). \quad \textbf{(1)}$$

Here $\hat{a}_s$ and $\hat{a}_i$ are the destruction operators of the signal and idler photons, respectively, κ is a coupling coefficient, and $\Delta k_z = k_p \cos(\theta_p) - k_s \cos(\theta_s) - k_i \cos(\theta_i)$ is the phase mismatch in the z direction. θ_p, θ_s, and θ_i are the angles between the lattice planes and the wave vectors of the pump, signal, and idler, respectively. The frequency domain operators are related to their real domain counterparts by $\hat{a}_j(z, \boldsymbol{r}, t) = \int\int_{-\infty}^{\infty} \hat{a}_j(z, \boldsymbol{q}, \omega)\exp[-i(\boldsymbol{q}\cdot\boldsymbol{r} - \omega t)]\mathrm{d}\boldsymbol{q}\mathrm{d}\omega$, where $\boldsymbol{r} \equiv (x, y)$ and $\boldsymbol{q} \equiv (k_x, k_y)$, and they satisfy the commutation relations given by $[\hat{a}_j(z_1, \boldsymbol{q}_1, \omega_1), \hat{a}_k^\dagger(z_2, \boldsymbol{q}_2, \omega_2)] = \frac{1}{(2\pi)^3}\delta_{j,k}\delta(z_1 - z_2)\delta(\boldsymbol{q}_1 - \boldsymbol{q}_2)\delta(\omega_1 - \omega_2)$.

Assuming the low gain approximation, we solve Eq. (1) to obtain a transfer matrix for the nonlinear crystal. To proceed it is more convenient to express the output state of the crystal as a superposition of the vacuum state and the biphoton state, calculated from the transfer matrix

$$|\Psi\rangle = C|0\rangle + \iiiint \mathrm{d}\boldsymbol{q}_s \mathrm{d}\omega_s \mathrm{d}\boldsymbol{q}_i \mathrm{d}\omega_i \times f(\boldsymbol{q}_s, \omega_s, \boldsymbol{q}_i, \omega_i)\hat{a}_s^\dagger(\boldsymbol{q}_s, \omega_s)\hat{a}_i^\dagger(\boldsymbol{q}_i, \omega_i)|0\rangle. \quad \textbf{(2)}$$

Here C and $f(\boldsymbol{q}_s, \omega_s, \boldsymbol{q}_i, \omega_i)$ are the probability amplitudes to detect the vacuum state and the frequency domain biphoton state, respectively. The obtained biphoton probability amplitude is

$$f(\boldsymbol{q}_s, \omega_s, \boldsymbol{q}_i, \omega_i) = (2\pi)^3 \kappa L \exp\left(i\frac{\Delta k_z L}{2}\right)\mathrm{sinc}\left(\frac{\Delta k_z L}{2}\right) \times \delta[\boldsymbol{q}_i - (\boldsymbol{q}_p + \boldsymbol{G} - \boldsymbol{q}_s)]\delta[\omega_i - (\omega_p - \omega_s)], \quad \textbf{(3)}$$

where L is the crystal length.

Next, we consider the mirrors and the beam splitter. Multilayer devices comprise alternating layers of two materials with low and high refractive indices, which are deposited on a substrate [34]. Since in the x-ray regime the refractive indices of materials depend only on the densities of the electrons, high and low atomic number materials are chosen to maximize the refractive index difference between the layers. They are commonly denoted as the "absorber" and the "spacer," respectively, and their widths are indicated by d_a and d_s. The ratio factor is defined as $\Gamma \equiv d_a/d$, where d is the width of the bilayers.

We use Bragg's law with a correction for refraction [36] to find the necessary width of the bilayers for a specific wavelength and incidence angle. To estimate the required number of bilayers we use the recursive theory of multilayers [37]. It allows an analytical expression to be obtained for the intensity reflectivity of N bilayers, where the incident angle is equal to the Bragg angle, and the refractions and the reflections from the substrate are negligible [36]:

$$R = \tanh^2[2Nr\sin(\pi n\Gamma)]. \quad \textbf{(4)}$$

Here r is the amplitude reflectivity of the electric field at the interface between the absorber and the spacer, and n is the number of the Bragg peak. However, Eq. (4) provides only the reflectivity for a specific wavelength at the Bragg angle, while the SPDC photons contain many frequencies and angles. Thus, we calculate numerically the reflectivity and the transmission of the mirror and the beam splitter by using the multilayer matrix theory [38] for the number of layers we estimated.

Finally, we calculate the count rate of coincidences between the two output ports of the beam splitter by using [39]

$$R_C = S\iint \mathrm{d}\boldsymbol{u}\mathrm{d}\tau \times \langle\Psi|\hat{a}_2^\dagger(\boldsymbol{r}_2, t_2)\hat{a}_1^\dagger(\boldsymbol{r}_1, t_1)\hat{a}_1(\boldsymbol{r}_1, t_1)\hat{a}_2(\boldsymbol{r}_2, t_2)|\Psi\rangle. \quad \textbf{(5)}$$

Here S is the area of the pump beam at the input of the nonlinear crystal, $\boldsymbol{u} = \boldsymbol{r}_2 - \boldsymbol{r}_1$ is the distance between two detection points, $\tau = t_2 - t_1$ is the duration between the detections, and $\hat{a}_1$ and $\hat{a}_2$ are the destruction operators at the two output ports of the beam splitter.

We calculate the propagation of the operators through the system by using the transfer matrices of the multilayer devices and insert the result along with Eqs. (2) and (3) into Eq. (5). After a considerable but straightforward calculation we obtain

$$
\begin{aligned}
R_C = \frac{S}{(2\pi)^9}\iint \mathrm{d}\boldsymbol{q}\mathrm{d}\omega\big\{&|M_s(\boldsymbol{q}_{++},\omega)M_i(\boldsymbol{q}_{--},\omega_p-\omega)\\
&\times\varphi(\boldsymbol{q}_{++},\omega)|^2\big[|A(\boldsymbol{q}_{+-},\omega_p-\omega)D(\boldsymbol{q}_{-+},\omega)|^2\\
&+|B(\boldsymbol{q}_{-+},\omega)C(\boldsymbol{q}_{+-},\omega_p-\omega)|^2\big]+M_s(\boldsymbol{q}_{+-},\omega_p-\omega)\\
&\times M_s^*(\boldsymbol{q}_{++},\omega)M_i(\boldsymbol{q}_{-+},\omega)M_i^*(\boldsymbol{q}_{--},\omega_p-\omega)\\
&\times\varphi^*(\boldsymbol{q}_{++},\omega)\varphi(\boldsymbol{q}_{+-},\omega_p-\omega)\exp[i(\omega_p-2\omega)T]\\
&\times[A(\boldsymbol{q}_{++},\omega)B^*(\boldsymbol{q}_{-+},\omega)C^*(\boldsymbol{q}_{+-},\omega_p-\omega)\\
&\times D(\boldsymbol{q}_{--},\omega_p-\omega)+A^*(\boldsymbol{q}_{+-},\omega_p-\omega)\\
&\times B(\boldsymbol{q}_{--},\omega_p-\omega)C(\boldsymbol{q}_{++},\omega)D^*(\boldsymbol{q}_{-+},\omega)]\big\}.
\end{aligned}
\tag{6}
$$

Here $\varphi(\boldsymbol{q}_s,\omega_s)=\iint f(\boldsymbol{q}_s,\omega_s,\boldsymbol{q}_i,\omega_i)\mathrm{d}\boldsymbol{q}_i\mathrm{d}\omega_i$ is the biphoton probability amplitude, T is the delay between the biphotons, M_s and M_i are the amplitude reflectivities of the signal and idler mirrors, respectively, A, B, C, and D are the elements of the transfer matrix of the beam splitter, and $\boldsymbol{q}_{\pm\pm}\equiv(\pm k_x,\pm k_y)$.

To exhibit the feasibility of observing the effect, we consider a system based on parameters used in previous experiments [30]. The nonlinear crystal is a diamond crystal with a thickness of 0.8 mm, and we use the C(660) atomic planes for phase matching. The pump is at 21 keV, it deviates by 8 mdeg from the Bragg angle of 44.609 deg, and it is polarized in the scattering plane. The pump rate is 10^{13} photons/s, and the beam area is 0.4 mm^2. The coupling coefficient is estimated to be about 10^{-19} m^{-1} [30]. We set the central energy of the signal and idler as 10.5 keV, and the phase matching equation results in propagation angles of 0.976 deg and −0.976 deg relative to the optical axis in Fig. 1. The signal and idler have parallel polarizations due to this setup [30], as required for identicalness.

We first show the coincidence count rate spectrum at the output of the nonlinear crystal in Fig. 2. We choose an aperture of the detector of 0.4 deg, which limits the photon energies it accepts to 8.54 keV–12.89 keV due to the one-to-one relation between the energy and the propagation direction. The total rate is about 0.15 pairs/s and the bandwidth is 4.35 keV, which fits experiments [30].

Next, we consider the multilayer mirrors and beam splitter. Our goal is to show it is possible to design devices with sufficient

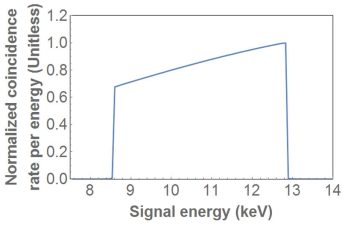

Fig. 2. Spectral dependence of the normalized coincidence count rate between the two output ports of the nonlinear crystal. The total bandwidth obtained for a detector aperture of 0.4 deg is 4.35 keV.

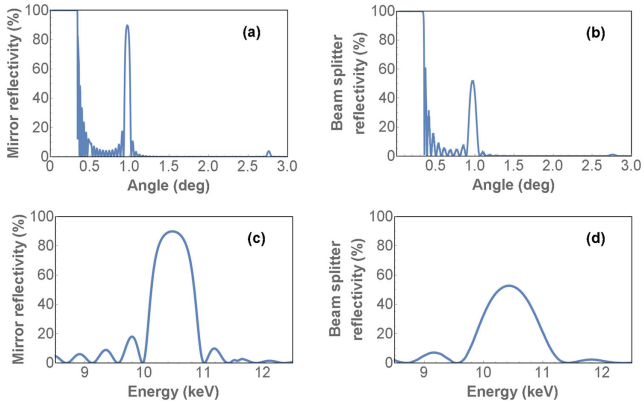

Fig. 3. Reflectivity of the mirrors and beam splitter versus the incidence angle, (a) and (b), and the photon energy, (c) and (d). Panels (a) and (c) show the mirror reflectivity and panels (b) and (d) show the beam splitter reflectivity. The bilayer width is 3.7 nm, with $\Gamma = 0.5$.

reflectivity to accommodate the broad angular distribution and spectrum of the biphotons. We choose the absorber and spacer layers to be platinum and carbon, respectively, and the substrates are a silicon wafer. We use the data from [40] for the refractive indices. By using Eq. (4) we find that 20 bilayers with a width of 3.7 nm and $\Gamma = 0.5$ are sufficient to achieve a 90% intensity reflectivity, and 10 bilayers suffice to achieve about 50% reflectivity. For the beam splitter, the substrate width is 15 μm, which is much shorter than the absorption length at 10.5 keV.

We simulate the dependence of the intensity reflectivity of the mirrors and the beam splitter on the incidence angle for 10.5 keV in Figs. 3(a) and 3(b). The high reflectivity at the lower angles is due to total reflection. We choose the first peak of the reflectivity at an incident angle of 0.976 deg, which is the incidence angle of the biphotons on the mirrors at perfect phase matching. The maximal reflectivity is 90%, and the FWHMs of the reflectivities of the mirror and the beam splitter are 0.07 deg and 0.095 deg, respectively. Figures 3(c) and 3(d) show the energy dependence of the reflectivity for an incident angle of 0.976 deg. The FWHM of the reflectivity of the mirror is 0.758 keV and of the beam splitter is 1.04 keV. As the angular acceptance and the bandwidth of the multilayer devices are comparable to those of the biphotons, our parameters enable observing reasonable count rates.

Now we turn to the main result of this Letter and calculate the FWHM of the coincidence count rate dip of x-ray HOM. We numerically calculate the integral described by Eq. (6) and show the result in Fig. 4, which is normalized to the output of the nonlinear crystal. The dip is nearly zero and its FWHM is about 0.6 attoseconds, which indicates a spectral bandwidth of 1.097 keV and an optical path difference between the biphotons of 1.8 angstroms.

We note that the energy bandwidth we calculated is wider than the bandwidth in Figs. 3(c) and 3(d), since the figures show the bandwidth for a specific incident angle, while the angular distribution of the biphotons is broad. This suggests the possibility to observe even shorter dips by designing multilayer devices with an angular dispersion that matches that of the biphotons. Also, we note that when the biphotons reach the beam splitter, one of them travels through the substrate first. This creates a small phase difference between the amplitude reflectivities of the beam splitter ports, which causes a shift in

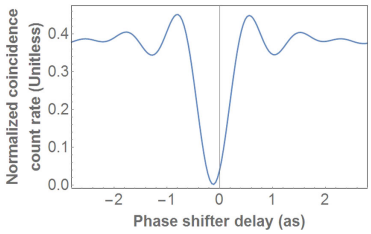

Fig. 4. Normalized coincidence count rate between the two output ports of the beam splitter versus the delay between the biphotons. The FWHM of the dip is about 0.6 attoseconds.

the coincidence count rate dip. Their indistinguishability is not destroyed though, as the intensity reflectivity is nearly equal for both sides.

We emphasize that while short optical path differences can be measured with x-ray interferometers [41–43], the HOM system exhibits an important advantage. Since in the HOM effect the interference is between wave functions instead of classical beams, incoherent sources can be used, while standard interferometers require sources with high spatial coherence.

Subattosecond delays can be achieved by placing a prism or thin films at the input of one of the interferometer arms. These components can introduce such delays since the refractive indices of many materials at x-ray wavelengths differ from the refractive index of air by only several of 10^{-6}. Hence, the optical path difference is subangstrom.

In conclusion, we have described how to implement the HOM effect for x-rays and utilize it to measure subattosecond time intervals and subangstrom optical path differences. The relaxed requirements for source coherence in comparison to interferometers suggest that the effect can be used for a large class of fundamental science measurements and applications. We note that our approach can be performed with present-day sources. New advanced sources such as the new high repetition rate free-electron lasers [44,45] would enhance the count rate significantly. In addition, the precision could be further improved by an order of magnitude via the approach described in Ref. [17]. Thus, our work opens the door for precision measurements supported by the ultra-high spatiotemporal precision that x-ray quantum effects enable.

Funding. Israel Science Foundation (201/17).

Disclosures. The authors declare no conflicts of interest.

REFERENCES

1. C. K. Hong, Z. Y. Ou, and L. Mandel, Phys. Rev. Lett. **59**, 2044 (1987).
2. Y. H. Shih and C. O. Alley, Phys. Rev. Lett. **61**, 2921 (1988).
3. J. G. Rarity, P. R. Tapster, E. Jakeman, T. Larchuk, R. A. Campos, M. C. Teich, and B. E. A. Saleh, Phys. Rev. Lett. **65**, 1348 (1990).
4. H. Lee, P. Kok, and J. P. Dowling, J. Mod. Opt. **49**, 2325 (2002).
5. C. Santori, D. Fattal, J. Vučković, G. S. Solomon, and Y. Yamamoto, Nature **419**, 594 (2002).
6. P. Walther, J.-W. Pan, M. Aspelmeyer, R. Ursin, S. Gasparoni, and A. Zeilinger, Nature **429**, 158 (2004).
7. J. Beugnon, M. P. A. Jones, J. Dingjan, B. Darquié, G. Messin, A. Browaeys, and P. Grangier, Nature **440**, 779 (2006).
8. Z.-Y. J. Ou, *Multi-Photon Quantum Interference* (Springer, 2007).
9. P. Kok, W. J. Munro, K. Nemoto, T. C. Ralph, J. P. Dowling, and G. J. Milburn, Rev. Mod. Phys. **79**, 135 (2007).
10. J. P. Dowling, Contemp. Phys. **49**, 125 (2008).
11. X. Ma, S. Zotter, J. Kofler, R. Ursin, T. Jennewein, Č. Brukner, and A. Zeilinger, Nat. Phys. **8**, 479 (2012).
12. L. A. Rozema, J. D. Bateman, D. H. Mahler, R. Okamoto, A. Feizpour, A. Hayat, and A. M. Steinberg, Phys. Rev. Lett. **112**, 223602 (2014).
13. J.-H. Kim, T. Cai, C. J. K. Richardson, R. P. Leavitt, and E. Waks, Optica **3**, 577 (2016).
14. J. S. Sidhu and P. Kok, Phys. Rev. A **95**, 063829 (2017).
15. E. Dauler, G. Jaeger, A. Muller, A. Migdall, and A. Sergienko, J. Res. Natl. Inst. Stand. Technol. **104**, 1 (1999).
16. D. Branning, A. L. Migdall, and A. V. Sergienko, Phys. Rev. A **62**, 063801 (2000).
17. A. Lyons, G. C. Knee, E. Bolduc, T. Roger, J. Leach, E. M. Gauger, and D. Faccio, Sci. Adv. **4**, eaap9416 (2018).
18. Y. Chen, M. Fink, F. Steinlechner, J. P. Torres, and R. Ursin, npj Quantum Inf. **5**, 1 (2019).
19. B. W. Adams, C. Buth, S. M. Cavaletto, J. Evers, Z. Harman, C. H. Keitel, A. Pálffy, A. Picón, R. Röhlsberger, Y. Rostovtsev, and K. Tamasaku, J. Mod. Opt. **60**, 2 (2013).
20. S. Shwartz, R. N. Coffee, J. M. Feldkamp, Y. Feng, J. B. Hastings, G. Y. Yin, and S. E. Harris, Phys. Rev. Lett. **109**, 013602 (2012).
21. R. Röhlsberger, H. C. Wille, K. Schlage, and B. Sahoo, Nature **482**, 199 (2012).
22. R. Röhlsberger, K. Schlage, B. Sahoo, S. Couet, and R. Ruffer, Science **328**, 1248 (2010).
23. F. Vagizov, V. Antonov, Y. V. Radeonychev, R. N. Shakhmuratov, and O. Kocharovskaya, Nature **508**, 80 (2014).
24. A. Schori, D. Borodin, K. Tamasaku, and S. Shwartz, Phys. Rev. A **97**, 063804 (2018).
25. S. Sofer, E. Strizhevsky, A. Schori, K. Tamasaku, and S. Shwartz, Phys. Rev. X **9**, 031033 (2019).
26. S. Shwartz and S. E. Harris, Phys. Rev. Lett. **106**, 080501 (2011).
27. R. Schützhold, G. Schaller, and D. Habs, Phys. Rev. Lett. **100**, 091301 (2008).
28. A. Pálffy, C. H. Keitel, and J. Evers, Phys. Rev. Lett. **103**, 017401 (2009).
29. C. C. Gerry and P. L. Knight, *Introductory Quantum Optics* (Cambridge University, 2004).
30. D. Borodin, A. Schori, F. Zontone, and S. Shwartz, Phys. Rev. A **94**, 013843 (2016).
31. A. F. Abouraddy, M. B. Nasr, B. E. A. Saleh, A. V. Sergienko, and M. C. Teich, Phys. Rev. A **65**, 053816 (2002).
32. M. B. Nasr, B. E. A. Saleh, A. V. Sergienko, and M. C. Teich, Opt. Express **12**, 1353 (2004).
33. D. Lopez-Mago and L. Novotny, Opt. Lett. **37**, 4077 (2012).
34. D. Attwood, *Soft X-Rays and Extreme Ultraviolet Radiation: Principles and Applications* (Cambridge University, 1999).
35. I. Freund and B. F. Levine, Phys. Rev. Lett. **23**, 854 (1969).
36. D. Spiga, "Development of multilayer-coated mirrors for future x-ray telescopes," Ph.D. thesis (University of Milano, 2004).
37. J. H. Underwood and T. W. Barbee, Appl. Opt. **20**, 3027 (1981).
38. B. E. A. Saleh and M. C. Teich, *Fundamentals of Photonics* (Wiley, 2007).
39. R. J. Glauber, Phys. Rev. **130**, 2529 (1963).
40. http://henke.lbl.gov/optical_constants/asf.html.
41. P. Becker and U. Bonse, J. Appl. Crystallogr. **7**, 593 (1974).
42. U. Bonse and M. Hart, Appl. Phys. Lett. **6**, 155 (1965).
43. K. Tamasaku, M. Yabashi, and T. Ishikawa, Phys. Rev. Lett. **88**, 044801 (2002).
44. S. Serkez, G. Geloni, S. Tomin, G. Feng, E. V. Gryzlova, A. N. Grum-Grzhimailo, and M. Meyer, J. Opt. **20**, 024005 (2018).
45. R. W. Schoenlein, S. Boutet, M. P. Minitti, and A. M. Dunne, Appl. Sci. **7**, 850 (2017).